

Measurements-Based Channel Models for Indoor LiFi Systems

Mohamed Amine Arfaoui*, Mohammad Dehghani Soltani, Iman Tavakkolnia, Ali Ghrayeb, Chadi Assi, Majid Safari, and Harald Haas

Abstract—Light-fidelity (LiFi) is a fully-networked bidirectional optical wireless communication (OWC) that is considered a promising solution for high-speed indoor connectivity. Unlike in conventional radio frequency wireless systems, the OWC channel is not isotropic, meaning that the device orientation affects the channel gain significantly. However, due to the lack of proper channel models for LiFi systems, many studies have assumed that the receiver is vertically upward and randomly located within the coverage area, which is not a realistic assumption from a practical point of view. In this paper, novel realistic and measurement-based channel models for indoor LiFi systems are proposed. Precisely, the statistics of the channel gain are derived for the case of randomly oriented stationary and mobile LiFi receivers. For stationary users, two channel models are proposed, namely, the modified truncated Laplace (MTL) model and the modified Beta (MB) model. For LiFi users, two channel models are proposed, namely, the sum of modified truncated Gaussian (SMTG) model and the sum of modified Beta (SMB) model. Based on the derived models, the impact of random orientation and spatial distribution of LiFi users is investigated, where we show that the aforementioned factors can strongly affect the channel gain and system performance.

Index Terms—Channel statistics, indoor channel models, light-fidelity (LiFi), Optical wireless communications, random waypoint, receiver orientation, receiver mobility.

I. INTRODUCTION

A. Motivation

The total data traffic is expected to become about 49 exabytes per month by 2021, while in 2016, it was approximately 7.24 exabytes per month [1]. With this drastic increase, the fifth generation (5G) networks and beyond must urgently provide high data rates, seamless connectivity, robust security and ultra-low latency communications [2]–[4]. In addition, with the emergence of the internet-of-things (IoT) networks, the number of connected devices to the internet is increasing dramatically [5], [6]. This fact implies not only a significant increase in data traffic, but also the emergence of some IoT services with crucial requirements. Such requirements include high data rates, high connection density, ultra reliable low latency communication (URLLC) and security. However, traditional radio-frequency (RF) networks, which are already

crowded, are unable to satisfy these high demands [7]. Network densification [8], [9] has been proposed as a solution to increase the capacity and coverage of 5G networks. However, with the continuous dramatic growth in data traffic, researchers from both industry and academia are trying to explore new network architectures, new transmission techniques and new spectra to meet these demands.

Light-fidelity (LiFi) is a novel bidirectional, high speed and fully networked wireless communication technology, that uses visible light as the propagation medium in the downlink for the purposes of illumination and communication. It can use infrared in the uplink so that the illumination constraint of a room remains unaffected, and also to avoid interference with the visible light in the downlink [10]. LiFi offers a number of important benefits that have made it favorable for future technologies. These include the very large, unregulated bandwidth available in the visible light spectrum (more than 2600 times greater than the whole RF spectrum), high energy efficiency [11], the straightforward deployment that uses off-the-shelf light emitting diode (LED) and photodiode (PD) devices at the transmitter and receiver ends, respectively, and enhanced security as light does not penetrate through opaque objects [12]. However, one of the key shortcomings of the current research literature on LiFi is the lack of appropriate statistical channel models for system design and handover management purposes.

B. Literature Review

Some statistical channel models for stationary and uniformly distributed users were proposed in [13]–[15], where a fixed incidence angle was assumed in [13], [14] and a random incidence angle was assumed in [15]. However, accounting for mobility, which is an inherent feature of wireless networks, requires a more realistic and non-uniform model for users' spatial distribution. Several mobility models, such as the random waypoint (RWP) model, have been proposed in the literature to characterize the spatial distribution of mobile users for indoor RF systems [16], [17]. However, these studies were limited to RF spectrum where statistical fading channel models were used. Recently, [18], [19] employed the RWP mobility model to characterize the signal-to-noise ratio (SNR) for indoor LiFi systems. In [18], the device orientation was assumed constant over time, which is not a realistic scenario, whereas in [19], the incidence angle of optical signals was assumed to be uniformly distributed, which is not a proper model for the incidence angle, since it does not account for the actual statistics of device orientation.

Device orientation can significantly affect the users'

M. A. Arfaoui and C. Assi are with Concordia Institute for Information Systems Engineering (CIISE), Concordia University, Montreal, Canada, e-mail: {m_arfaou@encs, assi@ciise}.concordia.ca.

M. D. Soltani, I. Tavakkolnia, M. Safari, and H. Haas are with the LiFi Research and Development Centre, Institute for Digital Communications, School of Engineering, University of Edinburgh, UK. e-mail: {m.dehghani, i.tavakkolnia, majid.safari, h.haas}@ed.ac.uk.

A. Ghrayeb is with the Electrical and Computer Engineering (ECE) department, Texas A&M University at Qatar, Doha, Qatar, e-mail: ali.ghrayeb@qatar.tamu.edu.

*Corresponding author: M.A. Arfaoui, m_arfaou@encs.concordia.ca

throughput. The majority of studies on OWC assume that the device always faces vertically upward. This assumption may have been driven by the lack of having a proper model for orientation, and/or to make the analysis tractable. Such an assumption is only accurate for a limited number of devices (e.g., laptops with a LiFi dongle), while the majority of users use devices such as smartphones, and in real-life scenarios, users tend to hold their device in a way that feels most comfortable. Such orientation can affect the users' throughput remarkably and it should be analyzed carefully. Even though a number of studies have considered the impact of random orientation in their analysis [20]–[27], all these studies assume a predefined model for the random orientation of the receiver. However, little or no evidence is presented to justify the assumed models. Nevertheless, none of these studies have considered the actual statistics of device orientation and have mainly assumed uniform or Gaussian distribution with hypothetical moments for device orientation. Recently, and for the first time, experimental measurements were carried out to model the polar and azimuth angles of the user's device in [28]–[31]. It is shown that the polar angle can be modeled by either a truncated Laplace distribution for the case of stationary users or a truncated Gaussian distribution for the case of mobile users, while the azimuth angle follows a uniform distribution for both cases. Motivated by these results, the impact of the random receiver orientation on the SNR and the bit error rate (BER) was studied for indoor stationary LiFi users in [32].

Solutions to alleviate the impact of device random orientation on the received SNR and throughput were proposed in [33]–[35]. In [33], the impact of the random receiver orientation, user mobility and blockage on the SNR and the BER was studied for indoor mobile LiFi users. Then, simulations of BER performance for spatial modulation using a multi-directional receiver configuration with consideration of random device orientation was evaluated. In [34], other multiple-input multiple-output (MIMO) techniques in the presence of random orientation were studied. The authors in [35], proposed an omni-directional receiver which is not affected by the device random orientation. It is shown that the omni-directional receiver reduces the SNR fluctuations and improves the user throughput remarkably. All these studies emphasize the significance of incorporating the random spatial distribution of LiFi users along with the random orientation of LiFi devices into the analysis. However, proper statistical channel models for indoor LiFi systems that encompass both the random spatial distribution and the random device orientation of LiFi users were not derived in the literature, which is the focus of this work.

C. Contributions and Outcomes

Against the above background, we investigate in this paper the channel statistics of indoor LiFi systems. Novel realistic and measurement-based channel models for indoor LiFi systems are proposed, and the proposed models encompass the random motion and the random device orientation of LiFi users. Precisely, the statistics of the line-of-sight (LOS) channel gain are derived for stationary and mobile LiFi users

with random device orientation, using the measurements-based models of device orientation derived in [28]. For stationary LiFi users, the model of randomly located user is employed to characterize the spatial distribution of the LiFi user, and the truncated Laplace distribution is used to model the device orientation. For mobile LiFi users, the RWP mobility model is used to characterize the spatial distribution of the user and the truncated Gaussian distribution is used to model the device orientation. In light of the above discussion, we may summarize the paper contributions as follows.

- For stationary LiFi users, two channel models are proposed, namely the modified truncated Laplace (MTL) model and the modified Beta (MB) model. For mobile LiFi users, also two channel models are proposed, namely the sum of modified truncated Gaussian (SMTG) model and the sum of modified Beta (SMB) model. The accuracy of the derived models is then validated using the Kolmogorov-Smirnov distance (KSD) criterion.
- The BER performance of LiFi systems is investigated for both cases of stationary and mobile users using the derived statistical channel models. We show that the random orientation and the random spatial distribution of LiFi users could have strong effect on the error performance of LiFi systems.
- We propose a novel design of indoor LiFi systems that can alleviate the effects of random device orientation and random spatial distribution of LiFi users. We show that the proposed design is able to guarantee good error performance for LiFi systems under the realistic behaviour of LiFi users.
- The proposed statistical LiFi channel models are of great significance. In fact, any LiFi transceiver design, to be efficient, it needs to incorporate the channel model into the design. Therefore, having realistic channel models will help in designing realistic LiFi transceivers.

Outline and Notations

The rest of the paper is organized as follows. The system model is presented in Section II. Section III presents the exact statistics of the LOS channel gain. In Sections IV, statistical channel models for stationary and mobile LiFi users are proposed. Finally, the paper is concluded in Section V and future research directions are highlighted.

The notations adopted throughout the paper are summarized in Table I. In addition, for every random variable X , f_X and F_X denote the probability density function (PDF) and the cumulative distribution function (CDF) of X , respectively. The function $\delta(\cdot)$ denotes the Dirac delta function. The function $\mathcal{U}_{[a,b]}(\cdot)$ denotes the the unit step function within $[a, b]$, i.e., for all $x \in \mathbb{R}$, $\mathcal{U}_{[a,b]}(x) = 1$ if $x \in [a, b]$, and 0 otherwise.

II. SYSTEM MODEL

Consider the indoor LiFi cellular system shown in Fig. 1, which consists of a LiFi attocell with radius R (green attocell), that is equipped with a single access-point (AP) installed at height h_a from the ground. The LiFi attocell is concentric with a larger circular area with a radius R_e ($R \leq R_e$), within

TABLE I
TABLE OF NOTATIONS

System Geometry	
R	Radius of the LiFi attocell
R_e	Radius of the large area
h_a	Height of the AP
h_u	Height of the LiFi receiver
LiFi Channel Parameters	
H	LOS channel gain
r	Polar distance of the LiFi user
α	Polar angle of the LiFi user
d	Distance from the AP to the LiFi user
Ω	Angle of the direction facing the LiFi user
θ	Elevation angle of the LiFi receiver
Ψ	Angle of incidence
Ψ_c	Field of view

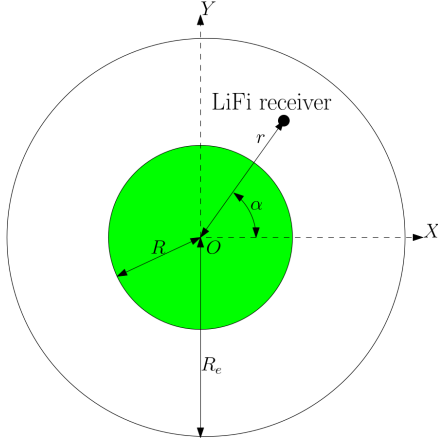


Fig. 1. Top view of a LiFi attocell which is concentric with a larger circular area.

which a LiFi user may be located. The user equipment (UE) is equipped with a single PD that is used for communication with the AP. Assuming that the global coordinate system (O, X, Y, Z) is cylindrical, the coordinates of the UE are given by (r, α, h_u) , where $r \in [0, R_e]$ is the polar distance, $\alpha \in [0, 2\pi]$ is the polar angle and $h_u \in [0, h_a]$ is the height of the LiFi receiver. The user is assumed to hold the UE within a close distance of the body. Therefore, the polar coordinates (r, α) of the UE are assumed exactly the same as those of the LiFi user. However, this is not the case for the height h_u , since it depends mainly on the activity of the LiFi user, i.e., either stationary (sitting activity) or mobile (walking activity). Furthermore, in this communication model, the UE can be connected to the AP if it is located inside the LiFi attocell, i.e., when $r \leq R$. In this case, the received signal at the LiFi receiver at each channel use is expressed as

$$Y = HS + N, \quad (1)$$

where H is the downlink channel gain, S is the transmitted signal and N is an additive white Gaussian noise (AWGN) that is $\mathcal{N}(0, \sigma^2)$ distributed. Since LiFi signals should be positive valued and satisfy a certain peak-power constraint [36], we assume that $0 \leq S \leq A$, where $A \in \mathbb{R}_+$ denotes the maximum

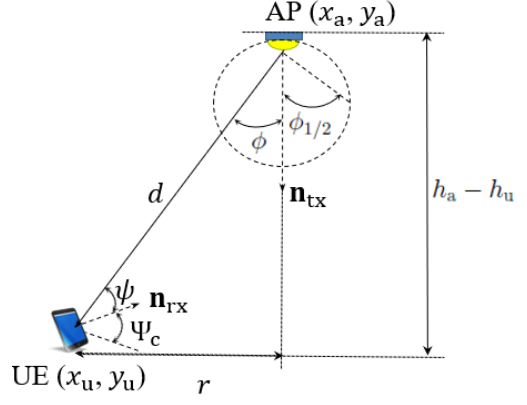


Fig. 2. Description of the indoor LiFi communication link.

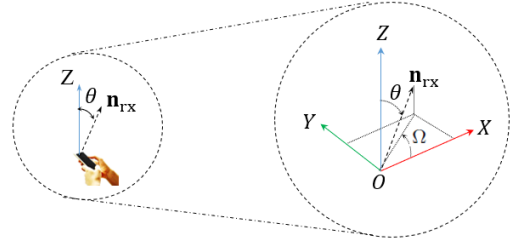


Fig. 3. Orientation angles of the LiFi receiver.

allowed signal amplitude.

The channel gain H is the sum of a LOS component and a non-light-of-sight (NLOS) component resulting from reflections of walls. However, it was observed in [37] that, for indoor LiFi scenarios, the optical power received from reflected signals is negligible compared to the LOS component, especially if the LiFi receiver is far away from the walls or is located close to the cell center. In this case, the contribution of the NLOS component is very small compared to that of the LOS component. Based on this, only the LOS component of H is considered, the channel gain H is expressed as [37]

$$H = H_0 \frac{\cos(\phi)^m \cos(\psi)}{d^2} \text{rect} \left(\frac{\psi}{\Psi_c} \right), \quad (2)$$

where, as shown in Fig. 2, m is the order of the Lambertian emission that is given by $m = \frac{-\log(2)}{\log(\cos(\phi_{1/2}))}$, such that $\phi_{1/2}$ represents the semi-angle of a LED; $d = \sqrt{r^2 + (h_a - h_u)^2}$ is the distance between the AP and the UE; $\phi \in [0, \phi_{1/2}]$ is the radiation angle; $\psi \in [0, \pi]$ is the incidence angle and Ψ_c is the field of view of the PD. In (2), H_0 is

$$H_0 = \rho R_p \frac{(m+1)}{2\pi} \frac{n_c^2 A_g}{\sin(\Psi_c)^2}, \quad (3)$$

where ρ is the electrical-to-optical conversion factor, R_p is the PD responsivity, A_g is the geometric area of the PD and n_c is the refractive index of the PD's optical concentrator.

Based on the results of [28], $\cos(\phi)$ and $\cos(\psi)$ are

expressed, respectively, as

$$\cos(\phi) = \frac{h_a - h_u}{d}, \quad (4a)$$

$$\cos(\psi) = \frac{(z_a - z_u)}{d} \cos(\theta) - \frac{(x_a - x_u)}{d} \cos(\Omega) \sin(\theta) - \frac{(y_a - y_u)}{d} \sin(\Omega) \sin(\theta), \quad (4b)$$

where (x_a, y_a, z_a) and (x_u, y_u, z_u) are the Cartesian coordinates of the AP and the UE, respectively, and as shown in Fig. 3, Ω and θ are the angle of direction and the elevation angle of the UE, respectively. The angle of direction Ω represents the angle between the direction the user is facing and the X -axis, whereas the elevation angle θ is the angle between the normal vector of PD n_{rx} and the Z -axis. Based on Fig. 2, we have $(x_a, y_a, z_a) = (0, 0, h_a)$ and $(x_u, y_u, z_u) = (r \cos(\alpha), r \sin(\alpha), h_u)$. Therefore, $\cos(\psi)$ can be expressed as

$$\cos(\psi) = \frac{r \cos(\Omega - \alpha) \sin(\theta) + (h_a - h_u) \cos(\theta)}{d}. \quad (5)$$

Consequently, the LOS channel gain H is expressed as

$$H = \left(\frac{a(\theta)r}{d^{m+3}} \cos(\Omega - \alpha) + \frac{b(\theta)}{d^{m+3}} \right) \times \mathbb{1}(\cos(\psi) > \cos(\Psi_c)), \quad (6)$$

where $a(\theta) = H_0(h_a - h_u)^m \sin(\theta)$ and $b(\theta) = H_0(h_a - h_u)^{m+1} \cos(\theta)$.

Based on the above, we conclude that the random behaviour of the channel gain H depends mainly on four random variables, which are r , α , Ω and θ . Precisely, the variables r and α model the randomness of the instantaneous location of the LiFi receiver whereas the variables Ω and θ model the randomness of the instantaneous UE orientation. Additionally, the statistics of the polar distance r and the elevation angle θ depend on the motion of the LiFi user, either stationary or mobile. Consequently, the statistics of the LOS channel gain H inducibly depend on the LiFi user activity. In the following section, the exact statistics of the channel gain H are derived for the case of stationary and mobile LiFi users.

III. CHANNEL STATISTICS OF STATIONARY AND MOBILE USERS WITH RANDOM DEVICE ORIENTATION

The objective of this section is deriving the exact statistics of the LOS channel gain H for the case of stationary and mobile LiFi users. In subsection III-A, we present the statistics of the four main factors r , α , Ω and θ for each case, from which we derive in subsection III-B the exact statistics of H .

A. Parameters Statistics

From a statistical point of view, the instantaneous location and the instantaneous orientation of the LiFi receiver are independent. Thus, the couples of random variables (r, α) and (Ω, θ) are independent. In addition, based on the results of [18], [38], the random variables r and α are independent, since r defines the polar distance and α defines the polar angle. On the other hand, based on the results of [28], the angle of direction Ω and the elevation angle θ are also statistically

independent. Therefore, the random variables r , α , Ω and θ are independent. In addition, for both cases of stationary and mobile LiFi users, the random variables α and Ω are uniformly distributed within $[0, 2\pi]$ [18], [28], [38]. However, this is not the case for the polar distance r and the elevation angle θ . In fact, as we will show in the following, the statistics of r and θ depend on whether the LiFi receiver is stationary or mobile.

1) Stationary Users:

When the LiFi user is stationary, its location is fixed. However, the LiFi user is randomly located, i.e., its instantaneous location is uniformly distributed within the circular area of radius R_e . In this case, the PDF of the polar distance r is expressed $f_r(r) = \frac{2r}{R_e^2} \mathcal{U}_{[0, R_e]}(r)$ [38]. Additionally, the authors in [28] presented a measurement-based study for the UE orientation, where they derived statistical models for the elevation angle θ . In this study, they show that, for stationary users, the elevation angle θ follows a truncated Laplace distribution, where its PDF is expressed as

$$f_\theta(\theta) = \frac{\exp\left(-\frac{|\theta - \mu_\theta|}{\sigma_\theta/\sqrt{2}}\right) \mathcal{U}_{[0, \pi/2]}(\theta)}{\sqrt{2}\sigma_\theta \left(1 - \exp\left(-\frac{\frac{\pi}{2} - \mu_\theta}{\sigma_\theta/\sqrt{2}}\right) - \exp\left(-\frac{\mu_\theta}{\sigma_\theta/\sqrt{2}}\right)\right)}, \quad (7)$$

such that $\mu_\theta = 41.39^\circ$ and $\sigma_\theta = 7.68^\circ$.

2) Mobile Users:

For mobile users, and especially in indoor environments, the UE motion represents the user's walk, which is equivalent to a 2-D topology of the RWP mobility model, where the direction, velocity and destination points (waypoints) are all selected randomly. Based on [16], [17], the spatial distribution of the LiFi receiver is polynomial in terms of the polar distance r and its PDF is expressed as $f_r(r) = \sum_{i=1}^3 a_i \frac{r^{b_i}}{R_e^{b_i+1}} \mathcal{U}_{[0, R_e]}(r)$, where $[a_1, a_2, a_3] = \frac{1}{75}[324, -420, 96]$ and $[b_1, b_2, b_3] = [1, 3, 5]$. Moreover, it was shown in the same measurement-based study in [28] that, for mobile users, the elevation angle θ follows a truncated Gaussian distribution, where its PDF is expressed as

$$f_\theta(\theta) = \frac{2 \exp\left(-\frac{(\theta - \mu_\theta)^2}{2\sigma_\theta^2}\right) \mathcal{U}_{[0, \pi/2]}(\theta)}{\sqrt{2\pi}\sigma_\theta^2 \left(\text{erf}\left(\frac{\frac{\pi}{2} - \mu_\theta}{\sqrt{2}\sigma_\theta}\right) + \text{erf}\left(\frac{\mu_\theta}{\sqrt{2}\sigma_\theta}\right)\right)}, \quad (8)$$

such that $\mu_\theta = 29.67^\circ$ and $\sigma_\theta = 7.78^\circ$.

B. Channel Statistics

As stated in Section II, the LiFi receiver can be located anywhere inside the outer cell with radius R_e . However, it is connected to the desired AP if it is located inside the LiFi attocell, i.e., if $r \in [0, R]$. In other words, in order to have a communication link between the desired AP and the LiFi receiver, the only admitted values of the polar distance r should be within the range $[0, R]$. Due to this, we constrain the range of r to be $[0, R]$, and therefore, the exact PDF of the polar distance r becomes $\tilde{f}_r(r) = \frac{f_r(r)}{F_r(R) - F_r(0)} \mathcal{U}_{[0, R]}(r)$, where F_r denotes the CDF of r . Consequently, the PDF of the distance $d = \sqrt{r^2 + (h_a - h_u)^2}$ is given by

$$f_d(d) = \frac{d \times \tilde{f}_r\left(\sqrt{d^2 - (h_a - h_u)^2}\right)}{\sqrt{d^2 - (h_a - h_u)^2}} \mathcal{U}_{[d_{\min}, d_{\max}]}(d), \quad (9)$$

$$F_{\cos(\psi)}(\cos(\Psi_c)) = \int_{d_{\min}}^{d_{\max}} \int_0^{\frac{\pi}{2}} F_{\cos(\Omega-\alpha)} \left(\frac{d \cos(\Psi_c) - (h_a - h_u) \cos \theta}{\sin(\theta) \sqrt{d^2 - (h_a - h_u)^2}} \right) f_\theta(\theta) d\theta f_d(d) dd \quad (13)$$

$$g_H(h) = \int_{d_{\min}^*(h)}^{d_{\max}} \int_0^{\frac{\pi}{2}} \frac{d^{m+3}}{a(\theta) \sqrt{d^2 - (h_a - h_u)^2}} f_{\cos(\Omega-\alpha)} \left(\frac{d^{m+3} h - b(\theta)}{a(\theta) \sqrt{d^2 - (h_a - h_u)^2}} \right) f_\theta(\theta) f_d(d) d\theta dd \\ + v(h) \int_0^{\frac{\pi}{2}} J_H(\theta, d) f_\theta(\theta) f_d(d) d\theta dd, \quad (15)$$

where $d_{\min} = h_a - h_u$ and $d_{\max} = \sqrt{R^2 + (h_a - h_u)^2}$. On the other hand, consider the random variable $\cos(\Omega - \alpha)$ appearing in (6). Since Ω and α are independent and uniformly distributed within $[0, 2\pi]$ and using the PDF transformation of random variables, $\cos(\Omega - \alpha)$ follows the arcsine distribution within the range $[-1, 1]$. Thus, the PDF and CDF of $\cos(\Omega - \alpha)$ are expressed, respectively, as

$$f_{\cos(\Omega-\alpha)}(x) = \frac{1}{\pi \sqrt{1-x^2}} \mathcal{U}_{[-1,1]}(x), \quad (10)$$

$$F_{\cos(\Omega-\alpha)}(x) = \left(\frac{\arcsin(x)}{\pi} + \frac{1}{2} \right) \mathcal{U}_{[-1,1]}(x) + \mathcal{U}_{[1,+\infty]}(x). \quad (11)$$

Based on this, the exact PDF of the channel gain H is given in the following theorem.

Theorem 1. *The range of the LOS channel gain H is $[h_{\min}, h_{\max}]$, where $h_{\min} = 0$ and $h_{\max} = \frac{H_0}{(h_a - h_u)^2}$. In addition, for $h \in [h_{\min}, h_{\max}]$, the PDF of H is expressed as*

$$f_H(h) = g_H(h) \mathcal{U}_{[h_{\min}^*, h_{\max}]}(h) + F_{\cos(\psi)}(\cos(\Psi_c)) \delta(h), \quad (12)$$

where $h_{\min}^* = \frac{H_0(h_a - h_u)^m \cos(\Psi_c)}{d_{\max}^{m+2}}$, $F_{\cos(\psi)}(\cos(\Psi_c))$ is given in (13) on top of this page, in which $d_{\min}^*(h) = \max(d_0(h), d_{\min})$ such that

$$d_0(h) = \left(\frac{h_0(h_a - h_u)^m \cos(\Psi_c)}{h} \right)^{\frac{1}{m+2}}. \quad (14)$$

and the function g_H is expressed as shown in (15) on top of this page, in which the function v is expressed as $v(h) = \frac{-(h_0(h_a - h_u)^m \cos(\Psi_c))^{\frac{m+3}{m+2}}}{d_{\max}^{\frac{m+3}{m+2}}} \mathcal{U}_{[h_{\min}^*, h_{\max}]}(h)$, such that $h_{\max}^* = \frac{H_0(h_a - h_u)^m \cos(\Psi_c)}{d_{\min}^{m+2}}$, and the function J_H is expressed as

$$J_H(\theta, d) = F_{\cos(\Omega-\alpha)} \left(\frac{d_{\min}^* \cos(\Psi_c) - (h_a - h_u) \cos(\theta)}{\sin(\theta) \sqrt{d_{\min}^{*2} - (h_a - h_u)^2}} \right) \\ - F_{\cos(\Omega-\alpha)} \left(\frac{d_{\min}^{*m+3} h - b(\theta)}{a(\theta) \sqrt{d_{\min}^{*2} - (h_a - h_u)^2}} \right). \quad (16)$$

Proof. See Appendix A. \square

The exact CDF of the LOS channel gain H is also provided in (40) in Appendix A. On the other hand, note that the function

$h \mapsto F_{\cos(\psi)}(\cos(\Psi_c)) \delta(h)$ expresses the effect of the field of view Ψ_c on the LOS channel gain H .

As it can be seen in Theorem 1, the closed-form expression of the exact PDF of the LOS channel gain H in (12) is neither straightforward nor tractable, since it involves some complex and atypical integrals. Due to this, in order to provide simple and tractable channel models for indoor LiFi systems, we propose in the following section some approximations for the PDF of H in (12), for the cases of stationary and mobile LiFi users.

IV. APPROXIMATE PDFS OF LiFi LOS CHANNEL GAIN

In this section, our objective is to derive some approximations for the PDF of H , starting from the results of Theorem 1. The cases of stationary and mobile LiFi users are investigated separately in subsections IV-A and IV-B, respectively.

A. Stationary Users

An approximate expression of the PDF of the LOS channel gain H for the case of stationary LiFi users is given in the following theorem.

Theorem 2. *For the case of stationary users, an approximate expression of the PDF of the channel gain H is given by*

$$f_H(h) \approx \frac{1}{h^\nu} g(h) + F_{\cos(\psi)}(\cos(\Psi_c)) \delta(h), \quad (17)$$

where $\nu > 0$ and g is a function with range $[h_{\min}^*, h_{\max}]$.

Proof. See Appendix B. \square

The approximation of the PDF of the LOS channel gain H provided in Theorem 2 expresses two main factors, which are the random location and random orientation of the UE. The functions $h \mapsto \frac{1}{h^\nu}$ and $h \mapsto g(h)$ express respectively the effects of the random location of the receiver and the random orientation of the UE on the LOS channel gain H . At this point, the missing part is the function g that provides the best approximation for the PDF of the LOS channel gain f_H . In the following, we provide two approximate expressions for the PDF g .

1) The Modified Truncated Laplace (MTL) Model:

Since the function $h \mapsto g(h)$ expresses the effect of the random orientation of UE on the LOS channel gain H and motivated by the fact that the elevation angle θ follows a truncated Laplace distribution as shown in (7), one reasonable choice for g is the Laplace distribution. Consequently, an

$$G_1(\gamma, \mu_H, b_H) = -b_H^{1+\gamma} e^{\frac{-\mu_H}{b_H}} \left[\Gamma\left(1 + \gamma, \frac{h_{\max}}{b_H}\right) - \Gamma\left(1 + \gamma, \frac{\mu_H}{b_H}\right) + (-1)^{1-\gamma} \left(\Gamma\left(1 + \gamma, -\frac{\mu_H}{b_H}\right) - \Gamma\left(1 + \gamma, -\frac{h_{\min}^*}{b_H}\right) \right) \right], \quad (20)$$

approximate expression of the PDF of the LOS channel gain H can be given by

$$f_H(h) \approx \frac{h^{-\nu} \exp\left(-\frac{|h-\mu_H|}{b_H}\right)}{M_1(-\nu, \mu_H, b_H)} \mathcal{U}_{[h_{\min}^*, h_{\max}]}(h) + F_{\cos(\psi)}(\cos(\Psi_c))\delta(h), \quad (18)$$

where $\mu_H \in [h_{\min}^*, h_{\max}]$, $b_H > 0$ and $M_1(-\nu, \mu_H, b_H)$ is a normalization factor given by

$$M_1(-\nu, \mu_H, b_H) = \frac{G_1(-\nu, \mu_H, b_H)}{[1 - F_{\cos(\psi)}(\cos(\Psi_c))]}, \quad (19)$$

where G_1 is given in (20) on top of this page, in which Γ denotes the upper incomplete Gamma function. At this stage, we need to determine the parameters (ν, μ_H, b_H) of f_H . One approach to do this is through moments matching. Using the exact PDF of H in (16), the non-centered moments of the LOS channel gain H are given by

$$m_i^e = \int_{h_{\min}^*}^{h_{\max}} h^i g_H(h) dh + F_{\cos(\psi)}(\cos(\Psi_c)), \quad i \in \mathbb{N}, \quad (21)$$

whereas by using the approximate PDF of H in (18), the non-centered moments of the LOS channel gain H are given by

$$m_i^a(\nu, \mu_H, b_H) = \frac{M_1(i - \nu, \mu_H, b_H)}{M_1(-\nu, \mu_H, b_H)}, \quad i \in \mathbb{N}, \quad (22)$$

Therefore, since only three parameters need to be determined, which are (ν, μ_H, b_H) , they can be obtained by solving the following system of equations

$$m_i^a(\nu, \mu_H, b_H) = m_i^e, \quad \text{for } i = 1, 2, 3. \quad (23)$$

2) The Modified Beta (MB) Model:

The exact PDF of the LOS channel gain H involves the integral of a function that has the form $(x, y) \mapsto f_{\cos(\Omega-\alpha)}(g(x, y))$. Since $\cos(\Omega - \alpha)$ follows the arcsine distribution and based on the fact that the arcsine distribution is a special case of the Beta distribution, we approximate the function g with a Beta distribution. Consequently, an approximate expression of the PDF of the LOS channel gain H can be given by

$$f_H(h) \approx \frac{h^{-\nu} \left(\frac{h-h_{\min}^*}{h_{\max}-h_{\min}^*}\right)^{\alpha_H-1} \left(\frac{h_{\max}-h}{h_{\max}-h_{\min}^*}\right)^{\beta_H-1}}{M_2(-\nu, \alpha_H, \beta_H)} \mathcal{U}_{[h_{\min}^*, h_{\max}]}(h) + F_{\cos(\psi)}(\cos(\Psi_c))\delta(h), \quad (24)$$

where $\alpha_H > 0$, $\beta_H > 0$ and $M_2(-\nu, \alpha_H, \beta_H)$ is a normalization factor given by

$$M_2(-\nu, \alpha_H, \beta_H) = \frac{G_2(-\nu, \alpha_H, \beta_H)}{[1 - F_{\cos(\psi)}(\cos(\Psi_c))]}, \quad (25)$$

such that G_2 is given in (26) at the top of the next page, in

which ${}_2\tilde{F}_1$ denotes the regularized hyper-geometric function and

$$B(\gamma, \alpha_H, \beta_H) = \frac{\pi h_{\max}^{\beta_H-1} (h_{\max} - h_{\min}^*)^{-\alpha_H-\beta_H+2}}{\sin(\pi(\alpha_H + \gamma))\Gamma(-\gamma)\Gamma(\alpha_H + \beta_H + \gamma)}. \quad (27)$$

Based on the above, it remains to derive the parameters (ν, α_H, β_H) of f_H . Similar to the case of the MTL model, one approach to do this is through moments matching. Specifically, (ν, α_H, β_H) can be obtained by solving the system of equations in (23), where for $i = 1, 2, 3$, m_i^a is expressed in this case as

$$m_i^a(\nu, \mu_H, b_H) = \frac{M_2(i - \nu, \alpha_H, \beta_H)}{M_2(-\nu, \alpha_H, \beta_H)}, \quad i \in \mathbb{N}. \quad (28)$$

B. Mobile Users

An approximate expression of the PDF of the LOS channel gain H for the case of mobile LiFi users is given in the following theorem.

Theorem 3. For the case of mobile users, an approximate expression of the PDF of the channel gain H is given by

$$f_H(h) \approx \sum_{j=1}^3 \frac{1}{h^{\nu_j}} g_j(h) + F_{\cos(\psi)}(\cos(\Psi_c))\delta(h), \quad (29)$$

where, for $j = 1, 2, 3$, $\nu_j > 0$ and g_j is a function with range $[h_{\min}^*, h_{\max}]$.

Proof. See Appendix C. \square

It is important to highlight here that, for $j = 1, 2, 3$, the functions $h \mapsto \frac{1}{h^{\nu_j}}$ and $h \mapsto g_j(h)$ express respectively the effects of user mobility and the random orientation of the UE on the LOS channel gain H . At this point, the missing part is the functions g_j , for $j = 1, 2, 3$, that provide the best approximation for the PDF of the LOS channel gain f_H . In the following, we provide two expressions for each function g_j for $j = 1, 2, 3$.

1) The Sum of Modified Truncated Gaussian (SMTG) Model:

Since for $j = 1, 2, 3$, the functions $h \mapsto g_j(h)$ express the effect of the random orientation of the UE on the channel gain H and motivated by the fact that, for the case of mobile LiFi users, the elevation angle θ follows a truncated Gaussian distribution as shown in (8), one reasonable choice for the functions g_j is the truncated Gaussian distribution. Consequently, an approximate expression of the PDF of the LOS channel gain H can be given by

$$f_H(h) \approx \frac{\sum_{j=1}^3 h^{-\nu_j} \exp\left(-\frac{(h-\mu_{H,j})^2}{2\sigma_{H,j}^2}\right)}{\sum_{j=1}^3 M_3(-\nu_j, \mu_{H,j}, \sigma_{H,j})} \mathcal{U}_{[h_{\min}^*, h_{\max}]}(h) + F_{\cos(\psi)}(\cos(\Psi_c))\delta(h), \quad (30)$$

$$G_2(\gamma, \alpha_H, \beta_H) = B(\gamma, \alpha_H, \beta_H) \times \left[\Gamma(\beta_H) \Gamma(-\gamma) h_{\max}^{\alpha_H + \gamma} {}_2\tilde{F}_1 \left(1 - \alpha_H, -\alpha_H - \beta_H - \gamma + 1; -\alpha_H - \gamma + 1; \frac{h_{\min}^*}{h_{\max}} \right) - \Gamma(\alpha_H) h_{\min}^{\alpha_H + \gamma} \Gamma(\alpha_H + \beta_H + \gamma) {}_2\tilde{F}_1 \left(1 - \beta_H, \gamma + 1; \beta_H + \gamma + 1; \frac{h_{\min}^*}{h_{\max}} \right) \right], \quad (26)$$

$$f_H(h) \approx \frac{\sum_{j=1}^3 h^{-\nu_j} \left(\frac{h - h_{\min}^*}{h_{\max} - h_{\min}^*} \right)^{\alpha_{H,j} - 1} \left(\frac{h_{\max} - h}{h_{\max} - h_{\min}^*} \right)^{\beta_{H,j} - 1} \mathcal{U}_{[h_{\min}^*, h_{\max}]}(h)}{\sum_{j=1}^3 M_2(-\nu_j, \alpha_{H,j}, \beta_{H,j})} + F_{\cos(\psi)}(\cos(\Psi_c)) \delta(h), \quad (34)$$

where for $j = 1, 2, 3$, $\mu_{H,j} \in [h_{\min}^*, h_{\max}]$, $\sigma_{H,j} > 0$ and $M_3(-\nu_j, \mu_{H,j}, \sigma_{H,j})$ is a normalization factor that is given by

$$M_3(-\nu_j, \mu_{H,j}, \sigma_{H,j}) = \frac{\int_{h_{\min}^*}^{h_{\max}} h^{-\nu_j} \exp\left(-\frac{(h - \mu_{H,j})^2}{2\sigma_{H,j}^2}\right) dh}{\left[1 - F_{\cos(\psi)}(\cos(\Psi_c))\right]}. \quad (31)$$

Now, in order to have the complete closed-form expression of f_H , we have to determine the parameters $\{\nu_j, \mu_{H,j}, \sigma_{H,j}\}$, $j = 1, 2, 3$. Similar to the one of the stationary users case, one approach to determine these parameters is through moments matching. Specifically, since only nine parameters need to be determined, which are $\{\nu_j, \mu_{H,j}, \sigma_{H,j} \mid j = 1, 2, 3\}$, they can be obtained by solving the following system of equations

$$m_i^a = m_i^e, \quad \text{for } i = 1, 2, \dots, 9, \quad (32)$$

where, for $i = 1, 2, \dots, 9$, m_i^a is expressed in this case as

$$m_i^a = \frac{\sum_{j=1}^3 M_3(i - \nu_j, \mu_{H,j}, \sigma_{H,j})}{\sum_{j=1}^3 M_3(-\nu_j, \mu_{H,j}, \sigma_{H,j})}. \quad (33)$$

2) The Sum of Modified Beta (SMB) Model:

Motivated by the same reasons as for the MB model in Section IV-A1, we approximate each function g_j , for $j = 1, 2, 3$, with a Beta distribution. Consequently, an approximate expression of the PDF of the LOS channel gain H is given in (34) at the top of this page, where $\alpha_{H,j} > 0$, $\beta_{H,j} > 0$ and $M_2(-\nu_j, \alpha_{H,j}, \beta_{H,j})$ is given in (25). Finally, it remains now to derive the parameters $\{\nu_j, \alpha_{H,j}, \beta_{H,j} \mid j = 1, 2, 3\}$ of f_H . Similar to the STMG model, these parameters can be obtained by solving the by solving the system of equations in (32), where for $i = 1, 2, \dots, 9$, m_i^a is expressed in this case as

$$m_i^a = \frac{\sum_{j=1}^3 M_2(i - \nu_j, \alpha_{H,j}, \beta_{H,j})}{\sum_{j=1}^3 M_2(-\nu_j, \alpha_H, \beta_H)}. \quad (35)$$

C. Summary of the Proposed Models

D. Summary of the Proposed Models

A detailed algorithm for implementing the proposed statistical channel models for indoor LiFi systems is presented in Algorithm 1.

Algorithm 1 Detailed algorithm for implementing the proposed statistical channel models

1. Input:

- i) Attocell dimensions (R, h_a) .
- ii) AP's parameters $(\rho, \phi_{1/2})$.
- iii) UE's height h_u
- iv) UE's parameters (R_p, n_c, A_g, Ψ_c) .

2. Calculate H_0 as shown in (3).

3. Calculate $F_{\cos(\psi)}(\cos(\Psi_c))$ as shown in (13).

4. If the LiFi user is stationary:

i) MTL model:

- a) Estimate the parameters using (23).
- b) Inject the parameters into the PDF in (18).

ii) MB model:

- a) Estimate the parameters using (23).
- b) Inject the parameters into the PDF in (24).

elseif the LiFi user is mobile:

i) SMTG model:

- a) Estimate the parameters using (32).
- b) Inject the parameters into the PDF in (30).

ii) SMB model:

- a) Estimate the parameters using (32).
- b) Inject the parameters into the PDF in (35).

end

TABLE II
SIMULATION PARAMETERS

Parameter	Symbol	Value
Ceiling height	h_a	2.4 m
LED half-power semiangle	$\phi_{1/2}$	60°
LED conversion factor	ρ	0.7 W/A
PD responsivity	R_p	0.6 A/W
PD geometric area	A_g	1 cm ²
Optical concentrator refractive index	n_c	1
UE's height (stationary)	h_u	0.9 m
UE's height (mobile)	h_u	1.4 m

V. SIMULATION RESULTS AND DISCUSSIONS

In this paper, we consider a typical indoor LiFi attocell [18], [19]. Parameters used throughout the paper are shown in Table II. In Subsection V-A, we present the PDF and CDF of the LOS channel gain H for the case of stationary

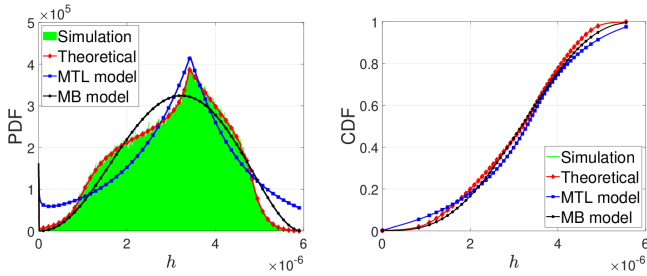
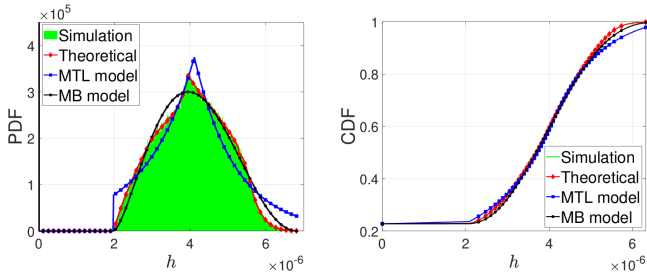
(a) PDF: $\Psi_c = 90^\circ$.(b) CDF: $\Psi_c = 90^\circ$.(c) PDF: $\Psi_c = 60^\circ$.(d) CDF: $\Psi_c = 60^\circ$.

Fig. 4. Comparison between the simulation, theoretical and approximation results of the PDF and the CDF of the LOS channel gain H for the case of stationary LiFi users when $R = 1\text{m}$.

and mobile LiFi users. In Subsection V-B, we investigate the error performance of Indoor LiFi systems using the derived statistics of the LOS channel gain H . Finally, based on the error performance presented in V-B, we propose in subsection V-C an optimized design for the indoor cellular system that can enhance the performance of LiFi systems.

A. Channel Statistics

For stationary LiFi users, Figs. 4 and 5 present the theoretical, simulated and approximated PDF and CDF of the LOS channel gain H , when a radius of the attocell of $R = 1\text{m}$ and $R = 2.5\text{m}$, respectively. For both cases, two different values for the field of view of the UE were considered, which are $\Psi_c = 90^\circ$ and 60° . These figures show that the proposed MTL and MB models offer good approximation for the distribution of the LOS channel gain H . Analytically, in order to evaluate the goodness of the proposed MTL and MB models, we use the well-known Kolmogorov-Smirnov distance (KSD) [39]. In fact, the KSD measures the absolute distance between two distinct CDFs F_1 and F_2 [39], i.e.,

$$\text{KSD} = \max_x |F_1(x) - F_2(x)|. \quad (36)$$

Obviously, smaller values of KSD correspond to more similarity between distributions. In our case, the KSD of the MTL and MB models are shown in Table III. As it can be seen in this table, the maximum KSD value for the MTL and MB models are 0.0669 and 0.0444, respectively, which demonstrates the good approximation offered by the MTL and MB models.

For mobile LiFi users, Figs. 6 and 7 present the theoretical, simulated and approximated PDF and CDF of the LOS channel gain H , when the radius of the attocell is $R = 1\text{m}$ and $R = 2.5\text{m}$, respectively. For both cases, two different values

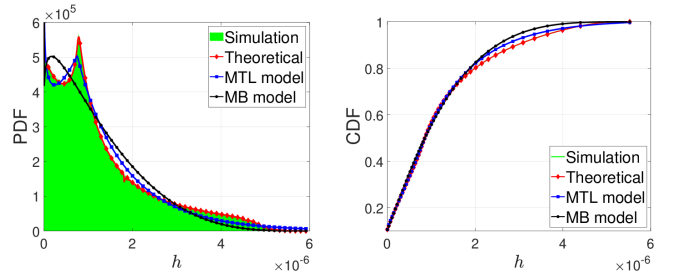
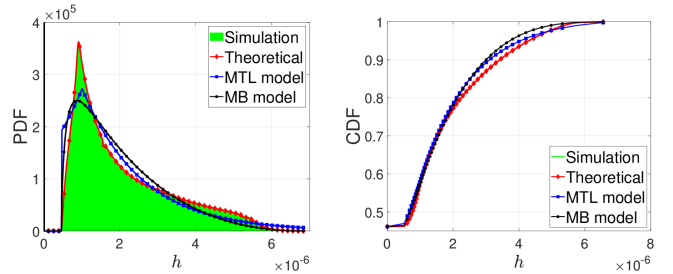
(a) PDF: $\Psi_c = 90^\circ$.(b) CDF: $\Psi_c = 90^\circ$.(c) PDF: $\Psi_c = 60^\circ$.(d) CDF: $\Psi_c = 60^\circ$.

Fig. 5. Comparison between the simulation, theoretical and approximation results of the PDF and the CDF of the LOS channel gain H for the case of stationary LiFi users when $R = 2.5\text{m}$.

TABLE III
KSD OF MTL AND MB MODELS

	MTL model		MB model	
	$\Psi_c = 90^\circ$	$\Psi_c = 60^\circ$	$\Psi_c = 90^\circ$	$\Psi_c = 60^\circ$
$R = 1\text{m}$	0.0669	0.0448	0.0336	0.0197
$R = 2.5\text{m}$	0.0239	0.0241	0.0444	0.0316

for the field of view of the UE were considered, which are $\Psi_c = 90^\circ$ and 60° . These figures show that the proposed SMTG and SMB models offer good approximation for the distribution of the LOS channel gain H . Furthermore, using the KSD metric, Table IV presents the KSD of the SMTG and the SMB models, where it shows that their maximum KSD values are 0.0238 and 0.0054, respectively. This result demonstrates the good approximation offered by the MTL and MB models.

B. Error Performance

Fig. 8 presents the average BER performance of the on-off keying (OOK) modulation versus the transmitted optical power P_{opt} for stationary and mobile users for the values of the attocell radius of $R = 1\text{m}$ and 2.5m and for the values of the field of view $\Psi_c = 90^\circ$ and $\Psi_c = 60^\circ$. Considering stationary users, this figure shows that the BER results of the MTL and MB models match perfectly the simulated BER for both cases when $(R, \Psi_c) = (2.5\text{m}, 90^\circ)$ and when $\Psi_c = 60^\circ$. However, for the case when $(R, \Psi_c) = (1\text{m}, 90^\circ)$, we remark that the average BER results of the MB model match the simulated BER better than the ones of the MTL model. This can be also seen from the values of the KSD in Table III, where we can see that the KSD of the MB model is lower

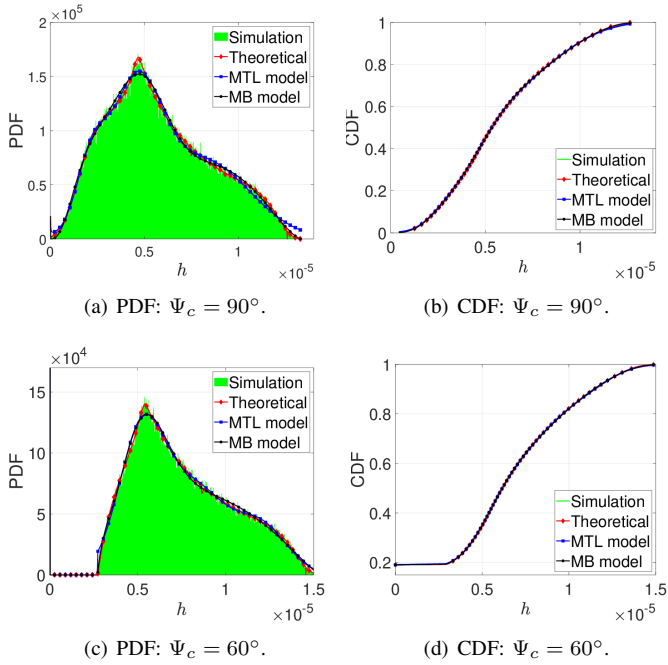


Fig. 6. Comparison between the simulation, theoretical and approximation results of the PDF and the CDF of the LOS channel gain H for the case of mobile LiFi users when $R = 2.5\text{m}$.

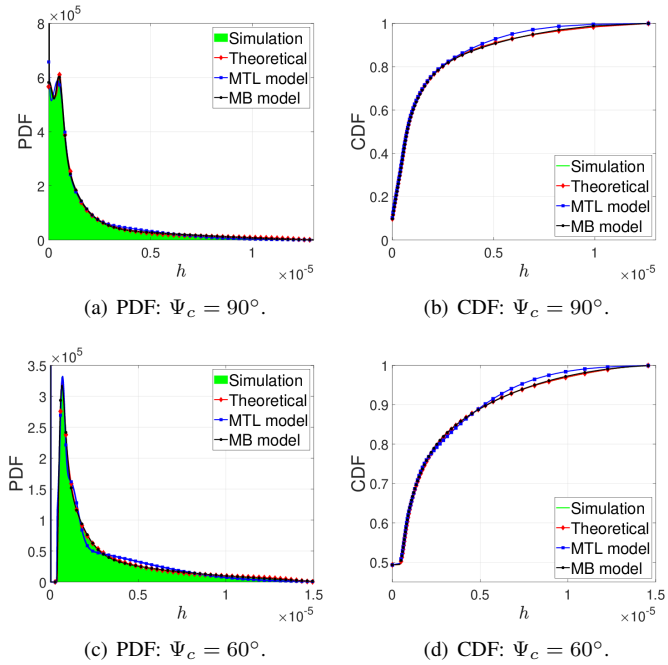


Fig. 7. Comparison between the simulation, theoretical and approximation results of the PDF and the CDF of the LOS channel gain H for the case of mobile LiFi users when $R = 2.5\text{m}$.

than the one of the MTL model when $(R, \Psi_c) = (1\text{m}, 90^\circ)$. In other words, when $(R, \Psi_c) = (1\text{m}, 90^\circ)$, the MB model offers better accuracy than the MTL model. This is mainly due to the assumptions made for both models. In fact, when the radius of the attocell R is small and by referring to (5), the random variable $\cos(\Omega - \alpha)$ is dominant in $\cos(\psi)$. Hence, assuming that the distribution of the random orientation

TABLE IV
KSD OF SMTG AND SMB MODELS

	MTL model		MB model	
	$\Psi_c = 90^\circ$	$\Psi_c = 60^\circ$	$\Psi_c = 90^\circ$	$\Psi_c = 60^\circ$
$R = 1\text{m}$	0.0082	0.0037	0.0048	0.0030
$R = 2.5\text{m}$	0.0238	0.0156	0.0054	0.0047

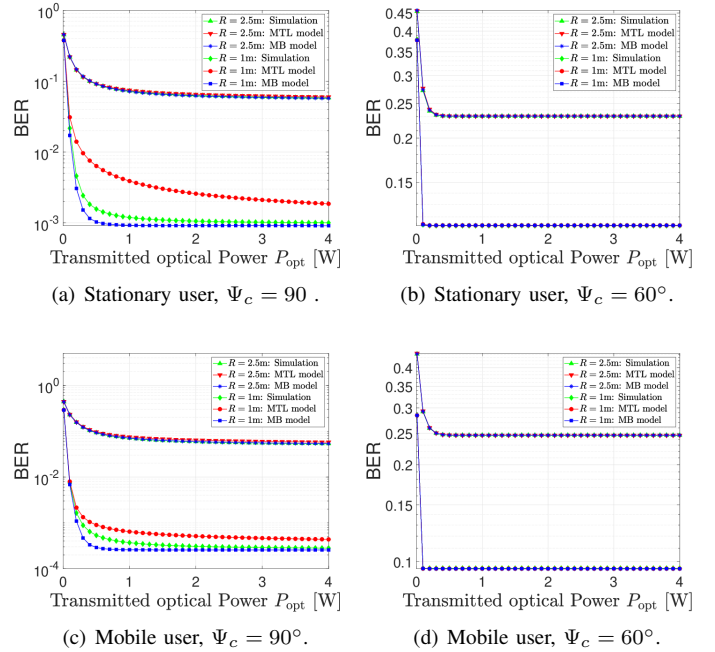


Fig. 8. BER performance of OOK modulation versus the transmitted optical power for stationary and mobile LiFi users.

of the UE can be approximated by a Beta distribution makes more sense. For mobile users, the same figure shows that the BER results of the SMTG and the SMB models match perfectly the simulated BER for both cases when $(R, \Psi_c) = (2.5\text{m}, 90^\circ)$ and when $\Psi_c = 60^\circ$. However, for the case when $(R, \Psi_c) = (1\text{m}, 90^\circ)$, we remark that the BER results of the SMB model matches the simulated BER better than the ones of the SMTG model. Similar to the case of stationary users, the SMB model offers better accuracy than the SMTG model when $(R, \Psi_c) = (1\text{m}, 90^\circ)$ due to the assumptions made for both models.

Fig. 8 shows also two important facts about the BER performance of LiFi users. First, it can be seen that the BER performance degrades heavily when either the radius of the attocell R increases or the field of view of the LiFi receiver decreases. Second, the BER saturates as the transmitted optical power increases. These two facts can be explained by the following corollary.

Corollary 1. At high transmitted optical power P_{opt} , the average probability of error of the M -ary pulse amplitude modulation (PAM) for the considered LiFi system is given by

$$\lim_{P_{\text{opt}} \rightarrow \infty} P_e(P_{\text{opt}}) = \frac{F_{\cos(\psi)}(\cos(\Psi_c))}{2}. \quad (37)$$

Proof. See appendix D. \square

The result of Corollary 1 shows that, even when the transmitted optical power P_{opt} is high, the BER is stagnating at $\frac{F_{\cos(\psi)}(\cos(\Psi_c))}{2}$. This result is directly related to the cases when the AP is out of the FOV of the LiFi receiver. On the other hand, based on its expression in (19), $F_{\cos(\psi)}(\cos(\Psi_c))$ is a function of the attocell radius R and the field of view of the receiver Ψ_c . Therefore, since d_{max} increases as R increases, then $F_{\cos(\psi)}(\cos(\Psi_c))$ is an increasing function in R . In addition, since $x \mapsto F_{\cos(\psi)}(x)$ is a CDF, it is an increasing function, and due to the fact that $x \mapsto \cos(x)$ is a decreasing function within $[0, \pi/2]$, then $F_{\cos(\psi)}(\cos(\Psi_c))$ increases as Ψ_c decreases. The aforementioned reasons explain the bad BER performance of the LiFi system when either the radius of the attocell R increases or the field of view Ψ_c decreases.

From a practical point of view, the above performance can be explained as follows. Recall that

$$F_{\cos(\psi)}(\cos(\Psi_c)) = \Pr(\cos(\psi) \leq \cos(\Psi_c)) \quad (38a)$$

$$= \Pr(H \leq 0), \quad (38b)$$

which is literally the outage probability of the LiFi system, i.e., the probability that the UE is not connected to the AP even when it is inside the attocell. Obviously, for large values of R or small values of Ψ_c , the probability that the LiFi receiver is not connected to the AP increases. This is mainly due to the effects the random location of the LiFi user along with the random orientation of the UE and it explains the bad BER performance in this case.

The question that may come to mind here is how can one enhance the performance of the LiFi system under such a realistic environment? Recently, some practical solutions have been proposed in the literature to alleviate the effects of the random behaviour of LiFi channel. These solutions include the use of MIMO LiFi systems along with transceiver designs that have high spatial diversity gains such as the multidirectional receiver (MDR) [33], [40], the omnidirectional transceiver [41] and the angular diversity transceiver [42]. In the following subsection, we propose a new design of indoor LiFi MIMO systems that can alleviate the effects of the random location of the LiFi user along with the random orientation of the UE.

C. Design Consideration of Indoor LiFi Systems

The concept of optical MIMO systems has been introduced in practical LiFi systems, where multiple LiFi APs cooperate together and serve multiple users within the resulting illuminated area [11], [34], [43], [44]. Each LiFi AP creates an optical attocell and the respective illumination areas of the adjacent attocells overlap with each other. Consider the indoor LiFi MIMO system shown in Fig. 9, which consists of five APs that correspond to small and adjacent attocells, where each has radius R_c . The distance between the AP of the attocell in the middle (green attocell), which we refer to as the reference attocell, and the APs of the remaining adjacent attocells is D_c .

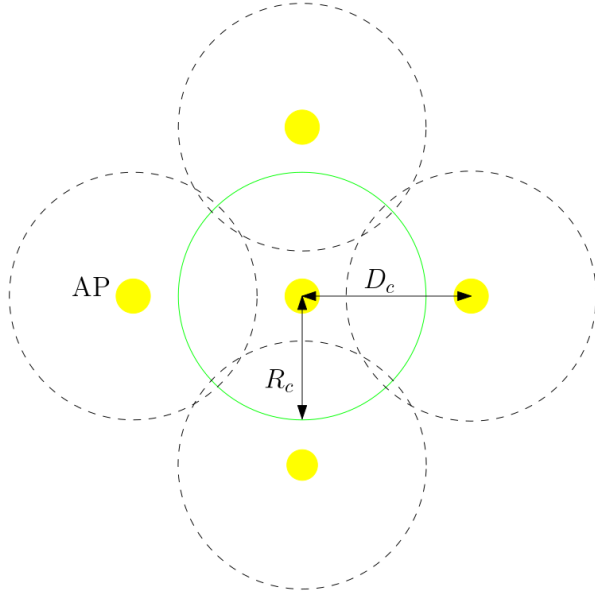
Let us assume that a LiFi user is located within the reference

attocell, where all five APs serve this user by transmitting the same signal. One way to reduce the outage probability of the LiFi user, i.e., the probability that it is not connected to one of the APs, is through a well designed attocells radius R_c and APs spacing D_c that guarantee a maximum target probability of error P_e^{th} , without any handover protocol or coordination scheme between the different APs. Fig. 10 presents the BER performance of a LiFi user that is located within the reference attocell, where the field of view of the UE is $\Psi_c = 60^\circ$. Both stationary and mobile cases are considered and different values of R_c and D_c are evaluated. By comparing the results of this figure and those of Fig. 8, for the case when $R = 1\text{m}$ for example, we can see how the coexisting APs can significantly improve the BER performance of the system. In addition, we remark from Fig. 10 that the choice of (R_c, D_c) has also a big impact on the BER performance, for example, for the case of a stationary user, the best choice among the considered values is $(R_c, D_c) = (1\text{m}, 1.5\text{m})$, whereas for the case of a mobile user, the best choice is $(R_c, D_c) = (1\text{m}, 1\text{m})$. Overall, for a target probability of error $P_e^{\text{th}} = 3.8 \times 10^{-3}$, we conclude that the choice $(R_c, D_c) = (1\text{m}, 1\text{m})$ is the best choice that guarantees the target performance jointly for both stationary and mobile users. Obviously, the optimal (R_c, D_c) depends on the geometry of the attocells and the parameters of the UE as well, such as the height of the AP h_a and the height of the UE h_u . This problem will be investigated in future works.

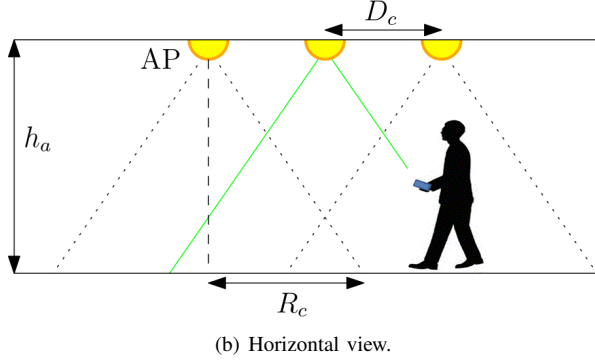
VI. CONCLUSIONS AND FUTURE WORKS

In this paper, novel, realistic, and measurement-based channel models for indoor LiFi systems have been proposed. The statistics of the LOS channel gain are derived for the case of stationary and mobile LiFi users, where the LiFi receiver is assumed to be randomly oriented. For stationary LiFi users, the MTL and the MB models were proposed, whereas for the case of mobile users, the SMTG and SMB models were proposed. The accuracy of each model was evaluated using the KSD. In addition, the effect of random orientation and spatial distribution of LiFi users on the error performance of LiFi users was investigated based on the derived models. Our results showed that the random behaviour and motion of LiFi users has strong effect on the LOS channel gain. Therefore, we proposed a novel design of indoor LiFi MIMO systems in order to guarantee the required reliability performance for reliable communication links.

The channel models proposed in this paper, albeit being fundamental and original, they serve as a starting point for developing realistic transmission techniques and transceiver designs tailored to real-world set-ups in an effort to bring the deployment of LiFi systems closer than ever. Thus, investigating optimal transceiver designs and cellular architectures based on the derived channel models that can meet the high demands of 5G and beyond in realistic communication environment can be considered as a future research direction. In addition, the derived channel models are intended for downlink communication in indoor LiFi environments. Therefore, deriving similar models for uplink transmission and for outdoor environments should also be considered in future work.



(a) Top view.



(b) Horizontal view.

Fig. 9. An indoor multi-cell LiFi system.

ACKNOWLEDGMENT

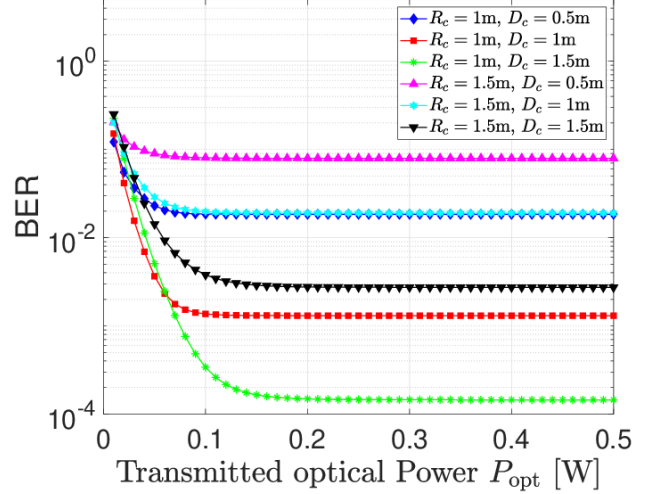
M. A. Arfaoui and C. Assi acknowledge the financial support from Concordia University and FQRNT. M. D. Soltani acknowledges the School of Engineering for providing financial support. A. Ghrayeb is supported in part by Qatar National Research Fund under NPRP Grant NPRP8-052-2-029 and in part by FQRNT. H. Haas acknowledges the financial support from the Wolfson Foundation and Royal Society. He also gratefully acknowledges financial support by the Engineering and Physical Sciences Research Council (EPSRC).

APPENDIX A PROOF OF THEOREM 1

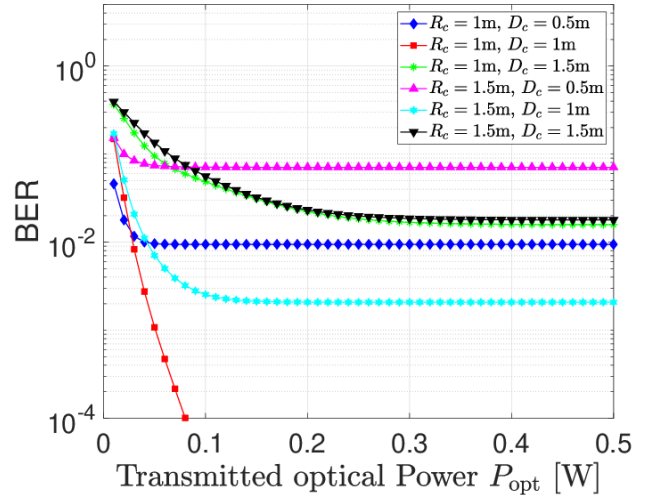
At first, let us determine the range of the LOS channel gain H . Recall that H is expressed as

$$H = H_0 \frac{(h_a - h_u)^m \cos(\psi)}{d^{m+2}} \times \mathbb{1}(\cos(\psi) > \cos(\Psi_c)), \quad (39)$$

where $\cos(\psi) = \frac{r \cos(\Omega - \alpha) \sin(\theta) + (h_a - h_u) \cos(\theta)}{d}$. Since $\Psi_c \in [0, \frac{\pi}{2}]$, we have $H \geq 0$ and the minimum value of H is equal to $h_{\min} = 0$. A set of values that can yield in $h_{\min} = 0$ is given as $d = d_{\min}$, $\Omega - \alpha = \pm k \frac{\pi}{2}$ s.t. $k = 1, 3$ and $\theta \geq \Psi_c$,



(a) Stationary user.



(b) Mobile user.

Fig. 10. BER performance of OOK modulation versus the transmitted optical power for stationary and mobile LiFi users when $\Psi_c = 60^\circ$.

which corresponds to the case where $\cos(\psi) \leq \cos(\Psi_c)$. On the other hand, the maximum value of H is equal to $h_{\max} = \frac{H_0}{(h_a - h_u)^2}$. A set of values that can yield in h_{\max} is expressed as $d = h_a - h_u$, $\Omega - \alpha = \pm \frac{\pi}{2}$ s.t. $k = 1, 3$ and $\theta = 0$, which corresponds to the case where $\cos(\psi) = 0$. On the other hand, the CDF of the LOS channel gain is expressed as shown in equation (40) on top of next page, where $a'(\theta) = \sin(\theta)$, $b'(\theta) = (h_a - h_u) \cos(\theta)$ and the function I_H is expressed as

$$I_H(\theta, d) = F_{\cos(\Omega - \alpha)} \left(\frac{d^{m+3} h - b(\theta)}{a(\theta) \sqrt{d^2 - (h_a - h_u)^2}} \right) - F_{\cos(\Omega - \alpha)} \left(\frac{d \cos(\Psi_c) - b'(\theta)}{a'(\theta) \sqrt{d^2 - (h_a - h_u)^2}} \right). \quad (41)$$

Equality (40g) follows from the fact that the conditional probability under the integral in (40f) is not null if and only

$$F_H(h) = \Pr(H \leq h) \quad (40a)$$

$$= \Pr \left(\left(a(\theta) \frac{\sqrt{d^2 - (h_a - h_u)^2}}{d^{m+3}} \cos(\Omega - \alpha) + \frac{b(\theta)}{d^{m+3}} \right) \times \mathbb{1}(\cos(\psi) > \cos(\Psi_c)) \leq h \right) \quad (40b)$$

$$= \Pr \left(a(\theta) \frac{\sqrt{d^2 - (h_a - h_u)^2}}{d^{m+3}} \cos(\Omega - \alpha) + \frac{b(\theta)}{d^{m+3}} \leq h, 0 \leq \psi \leq \Psi_c \right) + \Pr(0 \leq h, \Psi_c \leq \psi) \quad (40c)$$

$$= \Pr \left(a(\theta) \frac{\sqrt{d^2 - (h_a - h_u)^2}}{d^{m+3}} \cos(\Omega - \alpha) + \frac{b(\theta)}{d^{m+3}} \leq h, \cos(\Psi_c) \leq \cos(\psi) \right) + \Pr(0 \leq h, \cos(\psi) \leq \cos(\Psi_c)) \quad (40d)$$

$$= \int_{d_{\min}}^{d_{\max}} \int_0^{\frac{\pi}{2}} \Pr \left(\frac{d \cos(\Psi_c) - b'(\theta)}{a'(\theta) \sqrt{d^2 - (h_a - h_u)^2}} \leq \cos(\Omega - \alpha) \leq \frac{d^{m+3}h - b}{a(\theta) \sqrt{d^2 - (h_a - h_u)^2}} \middle| \theta, d \right) f_\theta(\theta) f_d(d) d\theta dd \quad (40e)$$

$$+ F_{\cos(\psi)}(\cos(\Psi_c)) \mathcal{U}_{[0, \infty]}(h) \\ = \int_{d_{\min}^*(h)}^{d_{\max}} \int_0^{\frac{\pi}{2}} I_H(\theta, d) f_\theta(\theta) f_d(d) d\theta dd + F_{\cos(\psi)}(\cos(\Psi_c)) \mathcal{U}_{[0, \infty]}(h), \quad (40f)$$

$$F_{\cos(\psi)}(\cos(\Psi_c)) = \Pr(\cos(\psi) \leq \cos(\Psi_c)) \quad (45a)$$

$$= \int_{d_{\min}}^{d_{\max}} \int_0^{\frac{\pi}{2}} \Pr(\cos(\psi) \leq \cos(\Psi_c) \middle| \theta, d) f_\theta(\theta) f_d(d) d\theta dd \quad (45b)$$

$$= \int_{d_{\min}}^{d_{\max}} \int_0^{\frac{\pi}{2}} \Pr \left(\cos(\Omega - \alpha) \leq \frac{d \cos(\Psi_c) - b'(\theta)}{a'(\theta) \sqrt{d^2 - (h_a - h_u)^2}} \middle| \theta, d \right) f_\theta(\theta) f_d(d) d\theta dd \quad (45c)$$

$$= \int_{d_{\min}}^{d_{\max}} \int_0^{\frac{\pi}{2}} F_{\cos(\Omega - \alpha)} \left(\frac{d \cos(\Psi_c) - (h_a - h_u) \cos(\theta)}{\sin(\theta) \sqrt{d^2 - (h_a - h_u)^2}} \right) f_\theta(\theta) f_d(d) d\theta dd. \quad (45d)$$

if

$$\frac{d \cos(\Psi_c) - b'(\theta)}{a'(\theta) \sqrt{d^2 - (h_a - h_u)^2}} \leq \frac{d^{m+3}h - b(\theta)}{a(\theta) \sqrt{d^2 - (h_a - h_u)^2}}, \quad (42)$$

i.e.,

$$\left(\frac{H_0(h_a - h_u)^m \cos(\Psi_c)}{h} \right)^{\frac{1}{m+2}} \leq d. \quad (43)$$

Or, d is constrained within the range $[d_{\min}, d_{\max}]$. Therefore, the conditional probability in (40e) is not null if and only if $d \in [d_{\min}^*(h), d_{\max}]$, where $d_{\min}^*(h) = \max(d_0(h), d_{\min})$ such that $d_0(h) = \left(\frac{H_0(h_a - h_u)^m \cos(\Psi_c)}{h} \right)^{\frac{1}{m+2}}$. Additionally, since d_0 should be always lower than d_{\max} , we conclude that the channel gain h under the integral in (50h) should satisfy $h_{\min}^* \leq h$, where

$$h_{\min}^* = \frac{H_0(h_a - h_u)^m \cos(\Psi_c)}{d_{\max}^{m+2}} \in [h_{\min}, h_{\max}]. \quad (44)$$

Furthermore, $F_{\cos(\psi)}(\cos(\Psi_c))$ in (40) is given as shown in (41) at the top of the next page. Based on this, the corresponding PDF of the LOS channel gain H is obtained by differentiating equality (40g) with respect to h . Using Leibniz integral rule for differentiation, the PDF of the LOS channel gain H is expressed as shown in (46) on the top of next page. for $h \in [h_{\min}^*, h_{\max}^*]$, and 0 otherwise, such that $h_{\max}^* = h_{\max} \cos(\Psi_c) \in [h_{\min}, h_{\max}]$. This completes the proof.

APPENDIX B PROOF OF THEOREM 2

Based on the results of Theorem 1, the PDF of the LOS channel gain H is given by

$$f_H(h) \\ = g_H(h) \mathcal{U}(h_{\min}^*, h_{\max}) + F_{\cos(\psi)}(\cos(\Psi_c)) \delta(h) \\ = (1 - F_{\cos(\psi)}(\cos(\Psi_c))) f_Z(h) + F_{\cos(\psi)}(\cos(\Psi_c)) \delta(h), \quad (47)$$

where f_Z is a PDF, with support range $[h_{\min}^*, h_{\max}^*]$. The PDF f_Z associated to a random variable Z that is expressed as $Z = XY$, where $X = \frac{c}{d^{m+2}}$ such that $c = H_0(h_a - h_u)^m$ and $Y = \cos(\psi)$ for $\psi \in [0, \Psi_c]$. Note that X and Y are two random variables that reflect the effects of the random spatial distribution of the LiFi user and the random orientation of the UE on the LOS channel gain, respectively. For the case of stationary users, and using the PDF transformation of random variables, the PDF of the random variable X is expressed as

$$f_X(x) = \frac{c^{\frac{1}{m+2}}}{(m+2)} \left(\frac{1}{x} \right)^{\frac{m+3}{m+2}} f_d \left(\left(\frac{c}{x} \right)^{\frac{1}{m+2}} \right) \\ = \frac{2c^{\frac{2}{m+2}}}{R^2(m+2)} \left(\frac{1}{x} \right)^{\frac{m+4}{m+2}} \mathcal{U}_{[c/d_{\max}^{m+2}, c/d_{\min}^{m+2}]}(x). \quad (48)$$

Obviously, X and Y are correlated since they are a function of the distance d , which is also a random variable. However, such correlation can be weak in most of the cases. In fact, for high values of d , the effect of random orientation on the

$$f_H(h) = \frac{\partial}{\partial h} [\Pr(H \leq h)] \quad (46a)$$

$$= \frac{\partial}{\partial h} \left[\int_{d_{\min}^*}^{d_{\max}} \int_0^{\frac{\pi}{2}} I_H(\theta, d) f_\theta(\theta) f_d(d) d\theta dd \right] + \frac{\partial}{\partial h} [F_{\cos(\psi)}(\cos(\Psi_c)) \mathcal{U}_{[0, \infty]}(h)] \quad (46b)$$

$$= \int_{d_{\min}^*}^{d_{\max}} \int_0^{\frac{\pi}{2}} \frac{d^{m+3}}{a(\theta) \sqrt{d^2 - (h_a - h_u)^2}} f_{\cos(\Omega - \alpha)} \left(\frac{d^{m+3} h - b(\theta)}{a(\theta) \sqrt{d^2 - (h_a - h_u)^2}} \right) f_\theta(\theta) f_d(d) d\theta dd \quad (46c)$$

$$+ v(h) \int_0^{\frac{\pi}{2}} J_H(\theta, d) f_\theta(\theta) d\theta + F_{\cos(\psi)}(\cos(\Psi_c)) \delta(h), \quad (46d)$$

LOS channel gain H is negligible compared to the one of the distance, whereas for the case of low values of d , the effect of distance is negligible compared to the one of random orientation. Due to this, as an approximation, we assume that the random variables X and Y are uncorrelated. Based on this, using the theorem of the PDF of the product of random variables [45], the PDF of the random variable Z can be approximated as

$$f_Z(h) \approx \int_{y_{\min}(h)}^{y_{\max}(h)} f_X\left(\frac{h}{y}\right) f_Y(y) \frac{dy}{y} \quad (49a)$$

$$= \int_{y_{\min}(h)}^{y_{\max}(h)} \frac{2c^{\frac{2}{m+2}}}{R^2(m+2)} \left(\frac{y}{h}\right)^{\frac{m+4}{m+2}} f_Y(y) \frac{dy}{y} \quad (49b)$$

$$= \left(\frac{1}{h}\right)^{\frac{m+4}{m+2}} \int_{y_{\min}(h)}^{y_{\max}(h)} \frac{2c^{\frac{2}{m+2}}}{R^2(m+2)} y^{\frac{2}{m+2}} f_Y(y) dy, \quad (49c)$$

where f_Y denotes the PDF of the random variable Y and it is given in (19) and (22) of [28]. Based on this, the PDF f_Z has the form

$$f_Z(h) \approx \frac{1}{h^\nu} \tilde{f}(h), \quad (50)$$

where $\nu > 0$ and \tilde{f} is a function with support range $[h_{\min}^*, h_{\max}]$ that is expressed as

$$\tilde{f}(h) = \int_{y_{\min}(h)}^{y_{\max}(h)} \frac{2c^{\frac{2}{m+2}}}{R^2(m+2)} y^{\frac{2}{m+2}} f_Y(y) dy. \quad (51)$$

Consequently, by substituting $f_Z(h)$ in (47) by its expression and defining the function g , for $h \in [h_{\min}^*, h_{\max}]$, as

$$g(h) = (1 - F_{\cos(\psi)}(\cos(\Psi_c))) \tilde{f}(h), \quad (52)$$

we obtain the result of Theorem 2, which completes the proof.

APPENDIX C PROOF OF THEOREM 3

Using the same notation adopted in Appendix B, the PDF of the random variable X for the case of mobile users is expressed as

$$\begin{aligned} f_X(x) &= \frac{c^{\frac{1}{m+2}}}{(m+2)} \left(\frac{1}{x}\right)^{\frac{m+3}{m+2}} f_d\left(\left(\frac{c}{x}\right)^{\frac{1}{m+2}}\right) \\ &= \sum_{i=1}^3 \frac{a_i c^{b_i + \frac{2}{m+2}}}{(m+2) R^{b_i+1}} \left(\frac{1}{x}\right)^{b_i + \frac{m+4}{m+2}} \mathcal{U}_{[c/d_{\max}^{m+2}, c/d_{\min}^{m+2}]}(x). \end{aligned} \quad (53)$$

Therefore, from (49b), the PDF of the random variable Z can be approximated by

$$\begin{aligned} f_Z(h) &\approx \int_{y_{\min}(h)}^{y_{\max}(h)} f_X\left(\frac{h}{y}\right) f_Y(y) \frac{dy}{y} \\ &= \sum_{i=1}^3 \left(\frac{1}{h}\right)^{b_i + \frac{m+4}{m+2}} \int_{y_{\min}(h)}^{y_{\max}(h)} \left[\frac{a_i c^{b_i + \frac{2}{m+2}}}{(m+2) R^{b_i+1}} \right. \\ &\quad \left. \times y^{b_i + \frac{m+4}{m+2}} f_Y(y) \right] dy, \end{aligned} \quad (54)$$

which has the form

$$f_Z(h) \approx \sum_{j=1}^3 \frac{1}{z^{\nu_j}} \tilde{f}_j(h), \quad (55)$$

where, for $j = 1, 2, 3$, $\nu_j > 0$ and \tilde{f}_j is a function with support range $[h_{\min}^*, h_{\max}]$ that is expressed as

$$\tilde{f}_j(h) = \int_{y_{\min}(h)}^{y_{\max}(h)} \left[\frac{a_i c^{b_i + \frac{2}{m+2}}}{(m+2) R^{b_i+1}} y^{b_i + \frac{m+4}{m+2}} f_Y(y) \right] dy. \quad (56)$$

Consequently, by substituting $f_Z(h)$ in (47) by its expression and defining $g_j(h)$, for $j = 1, 2, 3$ and for $h \in [h_{\min}^*, h_{\max}]$, as

$$g_j(h) = (1 - F_{\cos(\psi)}(\cos(\Psi_c))) \tilde{f}_j(h), \quad (57)$$

we obtain the result of Theorem 3, which completes the proof.

APPENDIX D PROOF OF COROLLARY 1

Based on PDF of the LOS channel gain H provided in Theorem 1 and the expression of the probability of error of M -pulse amplitude modulation [46]–[48], the average probability of error of the considered LiFi system is expressed as

$$P_e = \int_{h_{\min}}^{h_{\max}} f_H(h) P_{e,h}(P_{\text{opt}}, h) dh \quad (58a)$$

$$= \int_{h_{\min}}^{h_{\max}} f_H(h) \frac{2(M-1)}{M} \mathcal{Q}\left(\frac{h\sqrt{\gamma_{\text{TX}}}}{M-1}\right) dh \quad (58b)$$

$$= \int_{h_{\min}^*}^{h_{\max}} g_H(h) \frac{2(M-1)}{M} \mathcal{Q}\left(\frac{hP_{\text{opt}}}{\sigma(M-1)}\right) dh \quad (58c)$$

$$+ F_{\cos(\psi)}(\cos(\Psi_c)) \int_{h_{\min}}^{h_{\max}} \delta(h) \mathcal{Q}\left(\frac{hP_{\text{opt}}}{\sigma(M-1)}\right) dh,$$

where $P_{e,h}(P_{\text{opt}}, h)$ is the instantaneous probability of error for a given channel gain h and $\gamma_{\text{TX}} = \frac{P_{\text{elec}}}{\sigma^2} = \frac{P_{\text{opt}}^2}{\sigma^2}$ is the transmitted signal to noise ratio, such that P_{elec} is the transmitted signal to noise ratio and σ^2 is the average noise power at the receiver. Now, since the function $h \mapsto g_H(h) \frac{2(M-1)}{M} \mathcal{Q}\left(\frac{hP_{\text{opt}}}{\sigma(M-1)}\right)$ is a smooth function within $[h_{\text{min}}^*, h_{\text{max}}]$, and using the Lebesgue's dominated convergence theorem, we get

$$\begin{aligned} & \lim_{P_{\text{opt}} \rightarrow \infty} \int_{h_{\text{min}}}^{h_{\text{max}}} g_H(h) \frac{2(M-1)}{M} \mathcal{Q}\left(\frac{hP_{\text{opt}}}{\sigma(M-1)}\right) dh \\ &= \int_{h_{\text{min}}}^{h_{\text{max}}} \lim_{P_{\text{opt}} \rightarrow \infty} g_H(h) \frac{2(M-1)}{M} \mathcal{Q}\left(\frac{hP_{\text{opt}}}{\sigma(M-1)}\right) dh \\ &= 0. \end{aligned} \quad (59)$$

Furthermore, we have $\int_{h_{\text{min}}}^{h_{\text{max}}} \delta(h) \mathcal{Q}\left(\frac{hP_{\text{opt}}}{\sigma(M-1)}\right) dh = \mathcal{Q}(0) = \frac{1}{2}$ since $h_{\text{min}} = 0$, which implies that $\lim_{P_{\text{opt}} \rightarrow \infty} \int_{h_{\text{min}}}^{h_{\text{max}}} \delta(h) \mathcal{Q}\left(\frac{hP_{\text{opt}}}{\sigma(M-1)}\right) dh = \frac{1}{2}$. Therefore, we conclude that $\lim_{P_{\text{opt}} \rightarrow \infty} P_e(P_{\text{opt}}) = \frac{F_{\cos(\psi)}(\cos(\Psi_c))}{2}$, which completes the proof.

REFERENCES

- [1] C. V. Networking, "Cisco global cloud index: Forecast and methodology, 2016–2021," White Paper, Cisco, San Jose, CA, USA Nov. 2019.
- [2] J. G. Andrews, S. Buzzi, W. Choi, S. V. Hanly, A. Lozano, A. C. Soong, and J. C. Zhang, "What will 5G be?" *IEEE J. on selected areas in commun.*, vol. 32, no. 6, pp. 1065–1082, Jun. 2014.
- [3] M. Shafi, A. F. Molisch, P. J. Smith, T. Haustein, P. Zhu, P. Silva, F. Tufvesson, A. Benjebbour, and G. Wunder, "5G: A tutorial overview of standards, trials, challenges, deployment, and practice," *IEEE J. on selected areas in commun.*, vol. 35, no. 6, pp. 1201–1221, Apr. 2017.
- [4] P. Pirinen, "A brief overview of 5G research activities," in *Proc. IEEE 5GU*, Akasloppolo, Finland, Nov. 2014.
- [5] A. Al-Fuqaha, M. Guizani, M. Mohammadi, M. Aledhari, and M. Ayyash, "Internet of things: A survey on enabling technologies, protocols, and applications," *IEEE Commun. Surveys & Tutorials*, vol. 17, no. 4, pp. 2347–2376, Jun. 2015.
- [6] M. R. Palattella, M. Dohler, A. Grieco, G. Rizzo, J. Torsner, T. Engel, and L. Ladid, "Internet of things in the 5G era: Enablers, architecture, and business models," *IEEE J. on selected areas in commun.*, vol. 34, no. 3, pp. 510–527, Feb. 2016.
- [7] D. Tsonev, S. Videv, and H. Haas, "Towards a 100 Gb/s visible light wireless access network," *Optics express*, vol. 23, no. 2, pp. 1627–1637, Jan. 2015.
- [8] N. Bhushan, J. Li, D. Malladi, R. Gilmore, D. Brenner, A. Damjanovic, R. Sukhavasi, C. Patel, and S. Geirhofer, "Network densification: the dominant theme for wireless evolution into 5G," *IEEE Commun. Magazine*, vol. 52, no. 2, pp. 82–89, Feb. 2014.
- [9] X. Ge, S. Tu, G. Mao, C.-X. Wang, and T. Han, "5G ultra-dense cellular networks," *IEEE Wireless Commun.*, vol. 23, no. 1, pp. 72–79, Mar. 2016.
- [10] H. Haas, L. Yin, Y. Wang, and C. Chen, "What is lifi?" *Journal of lightwave technology*, vol. 34, no. 6, pp. 1533–1544, 2015.
- [11] I. Tavakkolnia, C. Chen, R. Bian, and H. Haas, "Energy-efficient adaptive mimo-vlc technique for indoor lifi applications," in *2018 25th International Conference on Telecommunications (ICT)*. IEEE, 2018, pp. 331–335.
- [12] S. Wu, H. Wang, and C.-H. Youn, "Visible light communications for 5G wireless networking systems: from fixed to mobile communications," *IEEE Network*, vol. 28, no. 6, pp. 41–45, Nov. 2014.
- [13] L. Yin, W. O. Popoola, X. Wu, and H. Haas, "Performance evaluation of non-orthogonal multiple access in visible light communication," *IEEE Trans. Commun.*, vol. 64, no. 12, pp. 5162–5175, Sep. 2016.
- [14] A. Gupta, N. Sharma, P. Garg, and M.-S. Alouini, "Cascaded FSO-VLC communication system," *IEEE Wireless Commun. Letters*, vol. 6, no. 6, pp. 810–813, 2Aug. 017.
- [15] Y. Yapici and I. Guvenc, "Non-orthogonal multiple access for mobile VLC networks with random receiver orientation," [Online]. Available: <https://arxiv.org/abs/1801.04888>, Jan. 2018.
- [16] K. Govindan, K. Zeng, and P. Mohapatra, "Probability density of the received power in mobile networks," *IEEE Trans. Wireless Commun.*, vol. 10, no. 11, pp. 3613–3619, Dec. 2011.
- [17] V. A. Aalo, C. Mukasa, and G. P. Efthymoglou, "Effect of mobility on the outage and BER performances of digital transmissions over Nakagami- m fading channels," *IEEE Trans. Vehicular Tech.*, vol. 65, no. 4, pp. 2715–2721, Apr. 2016.
- [18] A. Gupta and P. Garg, "Statistics of SNR for an indoor VLC system and its applications in system performance," *IEEE Commun. Letters*, vol. 22, no. 9, pp. 1898 – 1901, Jul. 2018.
- [19] M. A. Arfaoui, M. D. Soltani, I. Tavakkolnia, A. Ghayeb, C. Assi, H. Haas, M. Hasna, and M. Safari, "SNR Statistics for Indoor VLC Mobile Users with Random Orientation," in *Proc. IEEE ICC*, Shanghai, China, May. 2019.
- [20] M. Dehghani Soltani, X. Wu, M. Safari, and H. Haas, "Access point selection in li-fi cellular networks with arbitrary receiver orientation," in *2016 IEEE 27th Annual International Symposium on Personal, Indoor, and Mobile Radio Communications (PIMRC)*, Sep. 2016, pp. 1–6.
- [21] M. D. Soltani, H. Kazemi, M. Safari, and H. Haas, "Handover Modeling for Indoor Li-Fi Cellular Networks: The Effects of Receiver Mobility and Rotation," in *Proc. IEEE WCNC*, San Francisco, USA, Mar. 2017.
- [22] A. A. Purwita, M. D. Soltani, M. Safari, and H. Haas, "Handover probability of hybrid lifi/rf-based networks with randomly-oriented devices," in *2018 IEEE 87th Vehicular Technology Conference (VTC Spring)*, Porto, Portugal, June 2018, pp. 1–5.
- [23] J.-Y. Wang, Q.-L. Li, J.-X. Zhu, and Y. Wang, "Impact of receiver's tilted angle on channel capacity in vlcs," *Electronics Letters*, vol. 53, no. 6, pp. 421–423, 2017.
- [24] J.-Y. Wang, J.-B. Wang, B. Zhu, M. Lin, Y. Wu, Y. Wang, and M. Chen, "Improvement of ber performance by tilting receiver plane for indoor visible light communications with input-dependent noise," in *2017 IEEE International Conference on Communications (ICC)*. IEEE, 2017, pp. 1–6.
- [25] Z. Wang, C. Yu, W.-D. Zhong, and J. Chen, "Performance improvement by tilting receiver plane in m-qam ofdm visible light communications," *Optics express*, vol. 19, no. 14, pp. 13418–13427, 2011.
- [26] A. A. Matrawy, M. A. El-Shimy, M. R. Rizk, and Z. A. El-Sahn, "Optimum angle diversity receivers for indoor single user mimo visible light communication systems," in *Asia Communications and Photonics Conference*. Optical Society of America, 2016, pp. AS2C–4.
- [27] Y. S. Eroglu, Y. Yapici, and I. Guvenc, "Impact of random receiver orientation on visible light communications channel," *IEEE Transactions on Commun.*, vol. 67, no. 2, pp. 1313–1325, Nov. 2018.
- [28] M. D. Soltani, A. A. Purwita, Z. Zeng, H. Haas, and M. Safari, "Modeling the Random Orientation of Mobile Devices: Measurement, Analysis and LiFi Use Case," *IEEE Trans. Commun.*, vol. 67, no. 3, pp. 2157–2172, 2019.
- [29] A. A. Purwita, M. D. Soltani, M. Safari, and H. Haas, "Impact of terminal orientation on performance in LiFi systems," in *Proc. IEEE WCNC*, Barcelona, Spain, Apr. 2018.
- [30] Z. Zeng, M. D. Soltani, H. Haas, and M. Safari, "Orientation Model of Mobile Device for Indoor VLC and Millimetre Wave Systems," in *Proc. IEEE VTC*, Chicago, USA, Aug. 2018.
- [31] M. D. Soltani, "Analysis of Random Orientation and User Mobility in LiFi Networks," *The University of Edinburgh*, 2019.
- [32] M. D. Soltani, A. A. Purwita, I. Tavakkolnia, H. Haas, and M. Safari, "Impact of device orientation on error performance of LiFi systems," *IEEE Access*, vol. 7, pp. 41 690–41 701, 2019.
- [33] M. D. Soltani, M. A. Arfaoui, I. Tavakkolnia, A. Ghayeb, C. Assi, H. Haas, M. Hasna, and M. Safari, "Bidirectional optical spatial modulation for mobile users: Towards a practical design for lifi systems," *IEEE JSAC SI Spatial Modulation in Emerging Wireless Systems*, vol. 37, no. 9, pp. 2069 – 2086, Aug. 2019.
- [34] I. Tavakkolnia, M. D. Soltani, M. A. Arfaoui, A. Ghayeb, C. Assi, M. Safari, and H. Haas, "Mimo system with multi-directional receiver in optical wireless communications," in *2019 IEEE International Conference on Communications Workshops (ICC Workshops)*. IEEE, 2019, pp. 1–6.
- [35] C. Chen, M. D. Soltani, M. Safari, A. A. Purwita, X. Wu, and H. Haas, "An Omnidirectional User Equipment Configuration to Support Mobility in LiFi Networks," in *Proc. IEEE ICC*, Shanghai, China, May. 2019.
- [36] M.-A. Arfaoui, Z. Rezki, A. Ghayeb, and M. S. Alouini, "On the secrecy capacity of MISO visible light communication channels," in *Proc. IEEE Globecom*, Washington DC, USA, Dec. 2016.

- [37] L. Zeng, D. C. O'Brien, H. Le Minh, G. E. Faulkner, K. Lee, D. Jung, Y. Oh, and E. T. Won, "High data rate multiple input multiple output (MIMO) optical wireless communications using white led lighting," *IEEE JSAC*, vol. 27, no. 9, pp. 1654 – 1662, Dec. 2009.
- [38] M. A. Arfaoui, A. Ghayeb, and C. Assi, "Secrecy rate closed-form expressions for the SISO VLC wiretap channel with discrete input signaling," *IEEE Commun. Letters*, vol. 22, no. 7, pp. 1382 – 1385, Apr. 2018.
- [39] F. J. Massey Jr, "The kolmogorov-smirnov test for goodness of fit," *Journal of the American statistical Association*, vol. 46, no. 253, pp. 68–78, 1951.
- [40] I. Tavakkolnia, M. D. Soltani, M. A. Arfaoui, , A. Ghayeb, C. Assi, M. Safari, and H. Haas, "MIMO System with Multi-directional Receiver in Optical Wireless Communications," in *Proc. IEEE ICC*, Shanghai, China, May. 2019.
- [41] C. Chen, R. Bian, and H. Haas, "Omnidirectional transmitter and receiver design for wireless infrared uplink transmission in lifi," in *2018 IEEE International Conference on Communications Workshops (ICC Workshops)*. IEEE, 2018, pp. 1–6.
- [42] C. Chen, W.-D. Zhong, H. Yang, S. Zhang, and P. Du, "Reduction of sinr fluctuation in indoor multi-cell vlc systems using optimized angle diversity receiver," *Journal of Lightwave Technology*, vol. 36, no. 17, pp. 3603–3610, 2018.
- [43] T. Fath and H. Haas, "Performance comparison of MIMO techniques for optical wireless communications in indoor environments," *IEEE Trans. on Commun.*, vol. 61, no. 2, pp. 733–742, 2012.
- [44] M. D. Soltani, X. Wu, M. Safari, and H. Haas, "Bidirectional user throughput maximization based on feedback reduction in LiFi networks," *IEEE Trans. on Commun.*, vol. 66, no. 7, pp. 3172–3186, Feb. 2018.
- [45] A. G. Glen, L. M. Leemis, and J. H. Drew, "Computing the distribution of the product of two continuous random variables," *J. of Computational statistics & data analysis*, vol. 44, no. 3, pp. 451–464, Jan. 2004.
- [46] J. M. Kahn and J. R. Barry, "Wireless infrared communications," *Proc. of the IEEE*, vol. 85, no. 2, pp. 265–298, Feb. 1997.
- [47] P. Luo, Z. Ghassemlooy, H. Le Minh, E. Bentley, A. Burton, and X. Tang, "Fundamental analysis of a car to car visible light communication system," in *2014 9th International Symposium on Communication Systems, Networks & Digital Sign (CSNDSP)*. IEEE, 2014, pp. 1011–1016.
- [48] C.-C. Yeh and J. R. Barry, "Approximate minimum bit-error rate equalization for pulse-amplitude and quadrature-amplitude modulation," in *ICC'98. 1998 IEEE International Conference on Communications. Conference Record. Affiliated with SUPERCOMM'98 (Cat. No. 98CH36220)*, vol. 1. IEEE, 1998, pp. 16–20.